

Article

Design and Analysis of New Type of Magnetically Controlled Reactor

Yang Liu ^{1,2}, Fuyao Yang ^{1,2}, Yu Han ^{1,2,*}, Jie Gao ^{1,2}, Cong Wang ^{1,2}, Dezhi Chen ³  and Haonan Bai ³

¹ State Key Laboratory of Advanced Power Transmission Technology, Beijing 102209, China; liuyang_1@geiri.sgcc.com.cn (Y.L.); yangfuyao@geiri.sgcc.com.cn (F.Y.); gaojie@geiri.sgcc.com.cn (J.G.); wangcong@geiri.sgcc.com.cn (C.W.)

² State Grid Smart Grid Research Institute Co., Ltd., Beijing 102209, China

³ School of Electrical Engineering, Shenyang University of Technology, Shenyang 110870, China; chendezhi@sut.edu.cn (D.C.); baihaonan@smail.sut.edu.cn (H.B.)

* Correspondence: hanyu@geiri.sgcc.com.cn

Abstract: In recent years, various new types of magnetic materials have emerged, especially in the field of nanotechnology. The application of material composite technology has formed a new type of dual-phase composite magnetic material. Under the control of an external magnetic field, the material can achieve functional conversion between the hard magnetic phase and the soft magnetic phase, with magnetic permeability, non-magnetic permeability, and excitation ability. In this paper, it is proposed to use this material as the basic material for the magnetic state control of the reactor core, break through the bondage of the traditional reactor core to the performance of the controllable reactor, and innovatively form a new type of reactor structure. By adding a detection and control system, according to the working state of the power grid, the function conversion of the nano adjustable magnetic material is effectively adjusted to realize the automatic adjustment of the magnetic state of the reactor. Firstly, the preparation and material properties of dual-phase composite magnetic materials were studied. The design and preparation process from magnetic powder to bulk magnet were given, and the magnetic properties were measured. Secondly, a new 380 V/100 kVar magnetically controlled reactor was designed by using dual-phase composite magnetic material to form a composite core of magnetically controlled reactor on silicon steel sheet. The simulation analysis of electromagnetic characteristics and volt-ampere characteristics was carried out to verify the correctness of the proposed scheme.

Keywords: dual-phase composite magnetic material; preparation; magnetically controlled reactor; core



Citation: Liu, Y.; Yang, F.; Han, Y.; Gao, J.; Wang, C.; Chen, D.; Bai, H. Design and Analysis of New Type of Magnetically Controlled Reactor.

Energies **2024**, *17*, 2125. <https://doi.org/10.3390/en17092125>

Academic Editor: Mario Marchesoni

Received: 21 February 2024

Revised: 12 April 2024

Accepted: 17 April 2024

Published: 29 April 2024



Copyright: © 2024 by the authors. Licensee MDPI, Basel, Switzerland. This article is an open access article distributed under the terms and conditions of the Creative Commons Attribution (CC BY) license (<https://creativecommons.org/licenses/by/4.0/>).

1. Introduction

At present, the plan of building a strong smart grid is being put forward worldwide. The quality of power supply has become an important basis for evaluating the level of power grid operation together with the total power supply. The quality of power supply is not only the problem of voltage and frequency, but is also related to the safe and reliable operation of the power grid, related to energy conservation and environmental protection, and related to the strategic issues of sustainable development of the national economy [1].

In the process of modern industrial production, more and more power electronic converter devices are used, which will generate a large number of harmonics and inject non-sinusoidal currents into the power system. The load of a power grid is mainly inductive load (mainly motor), which forms lagging reactive power and has the characteristics of impact and imbalance. Whether from the point of view of maintaining the safe and stable operation of the power grid or from the point of view of improving the safe operation of the equipment, it is necessary to add a series of devices to the power grid to adjust and compensate the power indicators of the power grid. For example, the reactor is one of the effective devices, which is widely used to limit the power frequency overvoltage,

eliminate the self-excitation of the generator, limit the operating overvoltage, compensate the capacitive charging power of the line, suppress the secondary arc current, limit the short circuit, and stabilize the current. Theory and practice show that the regulation of reactance has a significant effect on improving the operation performance of power system, especially the application of a controllable reactor. Its capacity will automatically change with the size of transmission power, which can effectively prevent the switching overvoltage and the corresponding transient oscillation overvoltage generated when the switch on one side of the line is switched on, reduce the loss of the power grid, and improve the transmission energy, stability, and reliability of the power system.

In 1965, the British General Electric Company manufactured the world's first controllable reactor; from 1977 to 1978, American GE Company, Westinghouse Company, and BBC Company successively developed a thyristor-controlled static compensation device, an ultra-high voltage TCT type static compensation device, and a thyristor-controlled reactor (TCR); in 1986, the former Soviet Union proposed a new type of controllable reactor structure, so that the DC saturated controllable reactor would make a breakthrough, and the performance of the reactor would be greatly improved; in 1998, Japanese researchers proposed an orthogonal core controllable reactor based on the principle of controlled magnetic flux [2–5].

In recent years, scholars and research institutions have made achievements across many types of controllable reactors, such as controllable reactors based on PWM control, transformer-type controllable reactors based on controllable load principle, orthogonal core controllable reactors based on magnetic flux control principle, and ultra/ultra-high voltage controllable reactors [6–9].

As far as the current research and application are concerned, controllable reactors mainly include the following: the magnetic saturation controllable reactor, magnetic valve controllable reactor (MCR), high leakage reactance transformer controllable reactor (TCT), graded controllable shunt reactor, transformer controllable reactor (CRT), superconducting controllable reactor, etc. [10]. Among them, the outstanding advantages of the magnetically saturated controllable reactor are its suitability for high voltage level, relative stability, and low cost; on the other hand, it has a slow response speed. Although the magnetic valve controllable reactor has a fast response speed and a small network harmonic, its structure is more complex and commonly used in low-voltage lines [11]. The controllable reactor with high leakage reactance transformer has a simple structure, good response speed, continuity, and stability [12]. However, with the increase in capacity, the harmonic current injected into the system increases, and measures must be taken to control it, which increases the complexity of the system and reduces the reliability of the system [13]. The grading controllable reactor has the advantages of TCT controllable reactor, but its stability is poor. The transformer-type controllable reactor has the advantages of a small harmonic current and fast response speed, but it has a non-adjustable dead zone at light load, and the harmonic current analysis is also more complicated [14–20].

Table 1 shows a comparison of the characteristics of various controllable reactors.

It can be seen from the above analysis that although the existing controllable reactor can improve the operation performance of the power system, there are some problems in its own characteristics. Therefore, it is necessary to design a new type of controllable reactor to overcome the shortcomings of the existing controllable reactor and make its various indicators meet the requirements of power grid operation.

Based on previous studies, there is no effective method to establish an effective magnetic flux regulation mechanism inside the reactor core from the perspective of the design of the controllable reactor itself, and to realize the continuous adjustment of the reactance value of the controllable reactor.

Therefore, a two-phase composite magnetic material and its preparation method are proposed in this paper. Based on the magnetic properties of this material, it is applied to the magnetically controlled reactor. A 380 V/100 kvar new magnetically controlled reactor and its control system are designed. The relevant simulation and experimental research are carried out.

Table 1. Comparison of the characteristics of various controllable reactors.

Reactor	DC Magnetically Controlled	Switch Switching		Power Electronic Switch Controlled		Inverter Controlled
		Mechanical	Electronic	TCR	PCR	
reactance regulation	continuous	discontinuous		continuous		continuous
harmonics	serious	none		serious	none	none
response speed	slow	slow	fast	fast	faster	faster
loss, vibration noise	high noise	none		lower noise		lower noise
capacity	high	high	low	low	minimum	minimum
control precision	bad	worse		good	better	best
structural complexity	not so complex	easy		not so complex	relatively complicated	most complicated
cost	high	cheap	high	higher	higher	highest
saving energy				bad		

2. Preparation and Analysis of the Characteristics of Dual-Phase Composite Magnetic Materials

In this paper, the magnetic powder required for the properties of dual-phase composite magnetic materials was prepared by melting and rapid quenching. The magnetic powder composition was two alloys of $[\text{Nd}_{1-x}\text{La}_x]_8\text{Fe}_{86}\text{B}_6$ ($x = 0.3, 0.4$). The raw materials, Fe, Nd, La, and FeB alloys with a purity of 99.5%, were weighed according to the above composition and then melted in a WS-4 non-consumable vacuum arc melting furnace. The samples were repeatedly melted 5 times to ensure uniform composition. The melted samples were put into the strip cast machine at the roll speed of 25 m/s and 30 m/s, and the thin alloy strip was prepared. The technical method used is shown in Figure 1. The dual-phase composite magnetic material ribbons prepared by melting and rapid quenching are shown in Figure 2.

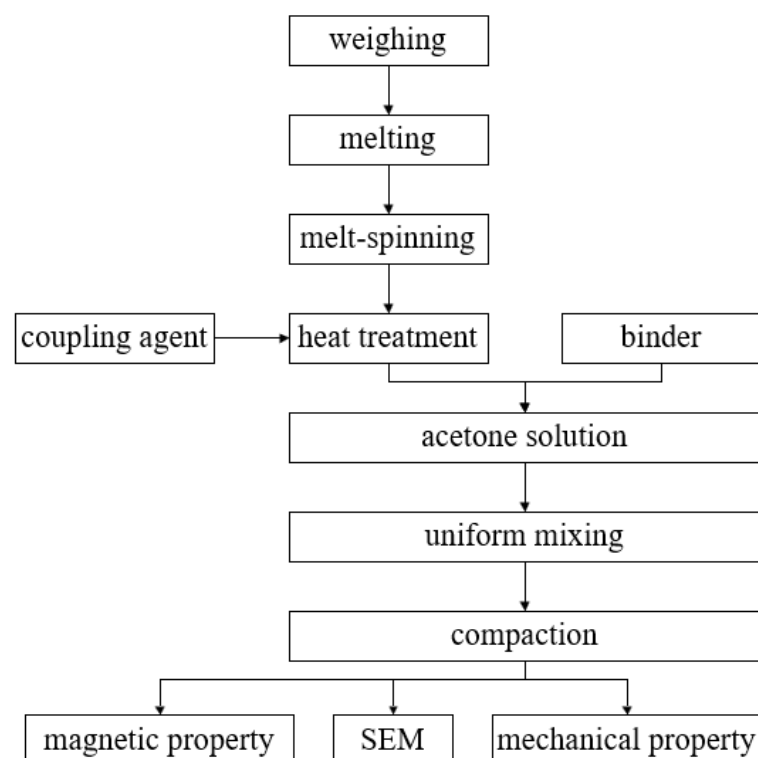
**Figure 1.** The technical method.



Figure 2. The dual-phase composite magnetic material ribbons prepared by melt-spinning method.

Figure 3 shows the magnetic testing equipment.



Figure 3. Magnetic testing equipment.

As shown in Figure 3, the measurement steps are as follows: First, turn on the power supply and test software, put the dual-phase composite magnetic material into the measuring device, and click measure to obtain the magnetic property curve of the dual-phase composite magnetic material as shown in Figure 4.

It can be seen from Figure 4 that the alloy is in the over-quenched state when the melt-spinning speed is 25 m/s and 30 m/s, and the remanence and coercivity are relatively low. When 30% La is substituted, the hysteresis loops at 25 m/s and 30 m/s are basically coincident, indicating that the magnetic properties are relatively stable at this time. When 40% La is substituted, the hysteresis loops are quite different, indicating that the phase composition and phase structure of the alloy ribbons are quite different. At 25 m/s roll speed, it can be seen from the shape of the initial magnetization curve that it is difficult to magnetize in the alloy at this time, which may be caused by more hard magnetic phases in the alloy at this roll speed. The large coercivity during demagnetization also indicates that there is a 2:14:1 hard magnetic phase in the alloy ribbon. When the roll speed is increased to 30 m/s, the alloy ribbons basically exhibit soft magnetic properties. This is because the alloy ribbons with increased roll speed are mainly composed of amorphous phases,

and due to the increase in La content, it is not conducive to the formation of 2:14:1 hard magnetic phase, so that more soft magnetic phases appear in the alloy. When 30% La is substituted, the saturation magnetization of the alloy at 25 m/s and 30 m/s roll speeds is 1.22 T and 1.24 T, respectively. When 40% La is substituted, the saturation magnetization of the alloy at 25 m/s and 30 m/s roll speeds is 1.38 T and 1.39 T, respectively. The increase in saturation magnetization may be due to the fact that La is not conducive to the formation of 2:14:1 hard magnetic phase, resulting in the increase in soft magnetic phase α -Fe. When 40% La is substituted, the maximum coercivity of 1708 Oe was obtained at 25 m/s.

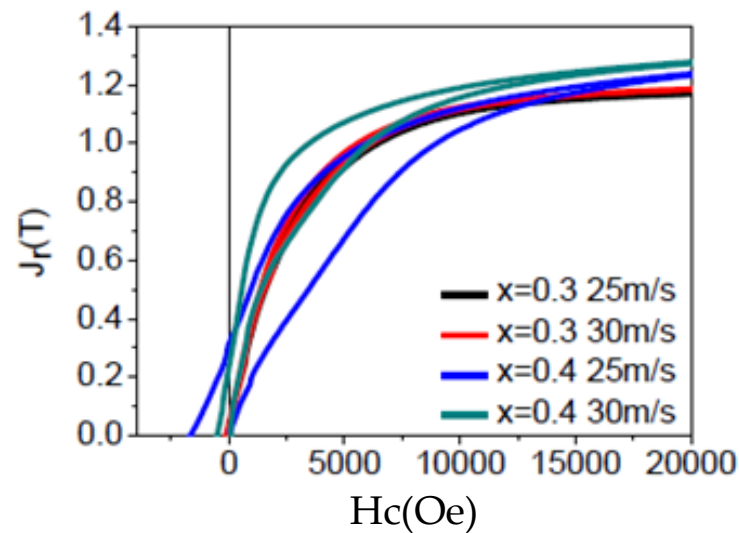


Figure 4. Magnetic property curves of dual-phase composite magnetic materials at different quenching speeds.

In order to obtain the best magnetic properties, the tape was subsequently heat-treated at 650 °C for 10 min. Figure 5 is the demagnetization curve of $[\text{Nd}_{1-x}\text{La}_x]_8\text{Fe}_{86}\text{B}_6$ ($x = 0.3, 0.4$) alloy ribbons after heat treatment at 650 °C for 10 min. It can be seen from the figure that the remanence and coercivity are improved after heat treatment, and the magnetic properties are shown in Table 2.

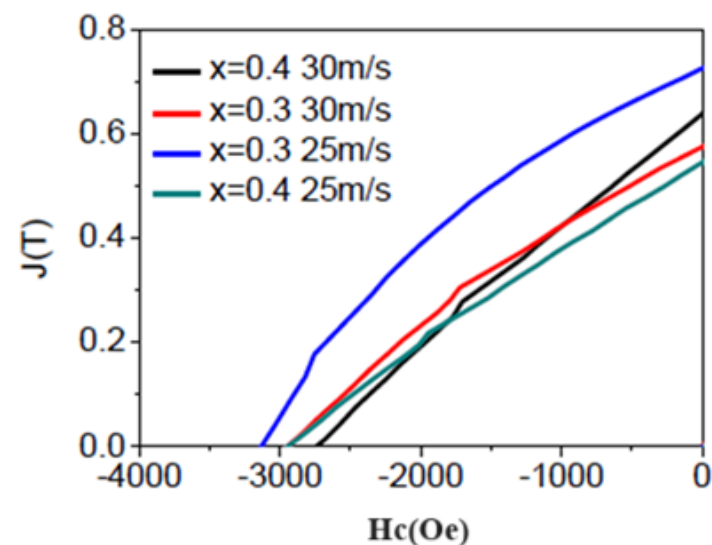


Figure 5. Demagnetization curve after heat treatment at 650 °C for 10 min.

Table 2. Magnetic properties of $[\text{Nd}_{1-x}\text{La}_x]_8\text{Fe}_{86}\text{B}_6$ ($x = 0.3, 0.4$) alloy ribbons after heat treatment at $650\text{ }^\circ\text{C}$ for 10 min.

	J_r (T)	H_c (Oe)	$(\text{BH})_{\text{max}}$ (kJ/m^3)
$x = 0.3$ 25 m/s	0.72	3133	42
$x = 0.3$ 30 m/s	0.57	2946	26
$x = 0.4$ 25 m/s	0.56	3130	26
$x = 0.4$ 30 m/s	0.64	2744	25

As shown in Table 2, when 30% La is substituted, the best magnetic properties can be obtained after heat treatment at a roll speed of 25 m/s. This is mainly due to the fact that the content of La is less at this time, and more NdFeB hard magnetic phases can be obtained. Because the intrinsic properties of NdFeB are higher than those of lanthanum iron boron, more excellent magnetic properties can be obtained at this time. And, lower roll speed is beneficial to obtain better microstructure, which is also an important reason for better performance. The roll speed was increased to 30 m/s; due to the increase in amorphous phase at this time, the hard magnetic phase obtained under the same conditions is less, which makes the performance decrease. When 40% La is substituted, the coercivity decreases from 3130Oe to 2744Oe with the increase in roll speed, which is also due to the increase in amorphous phase and the precipitation of less hard magnetic phase during heat treatment. At this time, the remanence at 30 m/s is higher than that at 25 m/s, indicating that the 30 m/s alloy ribbon contains more α -Fe soft magnetic phase during heat treatment.

In order to further reduce the coercivity, the alloy ribbons were heat treated at higher temperatures. The demagnetization curve of $[\text{Nd}_{1-x}\text{La}_x]_8\text{Fe}_{86}\text{B}_6$ ($x = 0.3, 0.4$) alloy ribbons after heat treatment at $850\text{ }^\circ\text{C}$ for 10 min is shown in Figure 6, and the magnetic properties are shown in Table 3. It can be seen from the figure that the coercivity of all samples is basically unchanged after heat treatment, and the remanence changes greatly. The coercivity is between 1250Oe and 1500Oe, which meets the project requirements. The coercivity ratio is lower than that at $650\text{ }^\circ\text{C}$ because the hard magnetic phase grains grow with the increase in heat treatment temperature, and the larger grains are easier to reverse magnetization during the demagnetization process and reduce the coercivity. It can be seen from the diagram that the remanence of 30% La substitution is higher than that of 40% La substitution, indicating that the increase in La content is not conducive to the precipitation of soft magnetic phase α -Fe. In the case of the same composition, the remanence of the alloy ribbon at 30 m/s is higher, indicating that the amorphous content obtained at higher roller speed is more, and more amorphous content makes it easier to form α -Fe phase during heating crystallization.

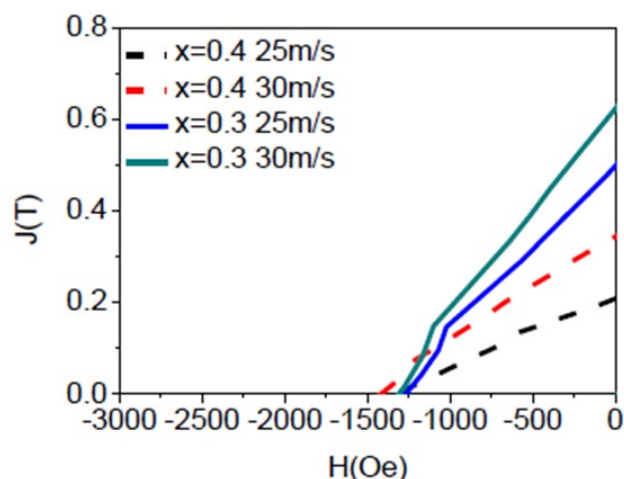
**Figure 6.** Demagnetization curve after heat treatment at $850\text{ }^\circ\text{C}$ for 10 min.

Table 3. Magnetic properties of $[\text{Nd}_{1-x}\text{La}_x]_8\text{Fe}_{86}\text{B}_6$ ($x = 0.3, 0.4$) alloy ribbons after heat treatment at $850\text{ }^\circ\text{C}$ for 10 min.

	J_r (T)	H_c (Oe)
$x = 0.3$ 25 m/s	0.50	1269
$x = 0.3$ 30 m/s	0.62	1310
$x = 0.4$ 25 m/s	0.21	1265
$x = 0.4$ 30 m/s	0.34	1424

Figure 7 shows the comparison of magnetic powder with binder and without binder. As shown in Figure 7, the coating property of magnetic powder is better after adding binder. It should be noted that the better the coating property of the magnetic powder, the better the compressive strength and magnetic properties.

**Figure 7.** Comparison of magnetic powder with binder and without binder.

After the magnetic powder is prepared, it is put into the mold and pressed on the hydraulic press, and the pressing pressure is 800 Mpa. The hydraulic press used in this experiment is shown in Figure 7, the shape of the mold and the magnet after pressing is shown in Figure 8, and the parameters of the magnet are shown in Table 4. From the diagram, it can be seen that 800 Mpa can successfully suppress the bulk magnet, and there are cracks on the side of the magnet when there is no adhesive, indicating that the bonding force of the magnet is not high after simple pressure. After adding the adhesive, the cracking of the magnet is basically eliminated to meet the required requirements.

Table 4. The main parameters of THP hydraulic press.

Item	Parameter
Nominal pressure	100 kN
Table area (mm^2)	500 mm \times 500 mm
Table height	700 mm
Work suppression	Pressure adjustable

Table 5 shows the main parameters of THP hydraulic press.

Table 5. Magnet parameters.

Long (mm)	Width (mm)	Hight (mm)	Volume (cm^3)	Mass (g)	Brinell Hardness (HBW)
56.5	10.1	11.2	6.39	33.73	24.6



Figure 8. Hydraulic press.

From Figure 9, it can be seen that the upper surface of the magnet after pressing is relatively flat, which is due to the smaller friction force on the upper surface during the forming and demolding process. However, the side of the magnet will have longitudinal scratches because of the large friction of the mold wall during demolding, and because the air in the powder is difficult to overflow during the pressing process, there will also be unevenness.



Figure 9. Shape of the mold and the magnet after pressing.

The magnetic properties of the prepared magnets were tested, and the test results are shown in Figure 10. It can be seen from the figure that the remanence of the magnet after bonding is reduced, and the coercivity is basically unchanged. This is because the density of the magnet after pressing is not high, there is a certain porosity, and a demagnetization field is formed in the magnet to reduce the remanence. The magnetic properties data are shown in Table 6.

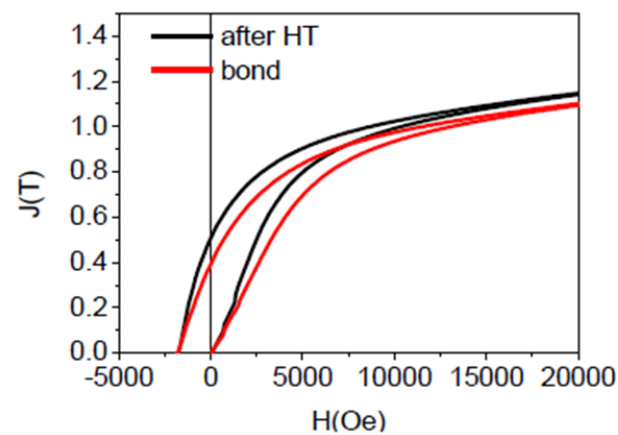


Figure 10. Comparison of magnetic properties before and after bonding.

Table 6. Magnetic properties value.

	J_r (T)	H_c (Oe)	$(BH)_{max}$ (kJ/m ³)
After HT	0.51	1750	16
Bond	0.39	1816	11

The prepared bonded magnet was tested by scanning electron microscopy. The surface test results of the magnet are shown in Figure 11, and the internal test results are shown in Figure 12. It can be seen that the surface of the magnet is relatively flat, the smaller magnet has a fracture situation, and there is a gap in the contact area of the powder edge. From the backscattering diagram, it can be seen that the brighter pattern is the NdFeB magnet, and the darker is the adhesive. It can be seen that the adhesive is distributed between the powder, which plays a certain connection role and increases the mechanical strength of the magnet. It can be seen in Figure 11 that the internal arrangement of the magnet is relatively close, and the distribution of the adhesive is more uniform, which can better increase the mechanical strength.

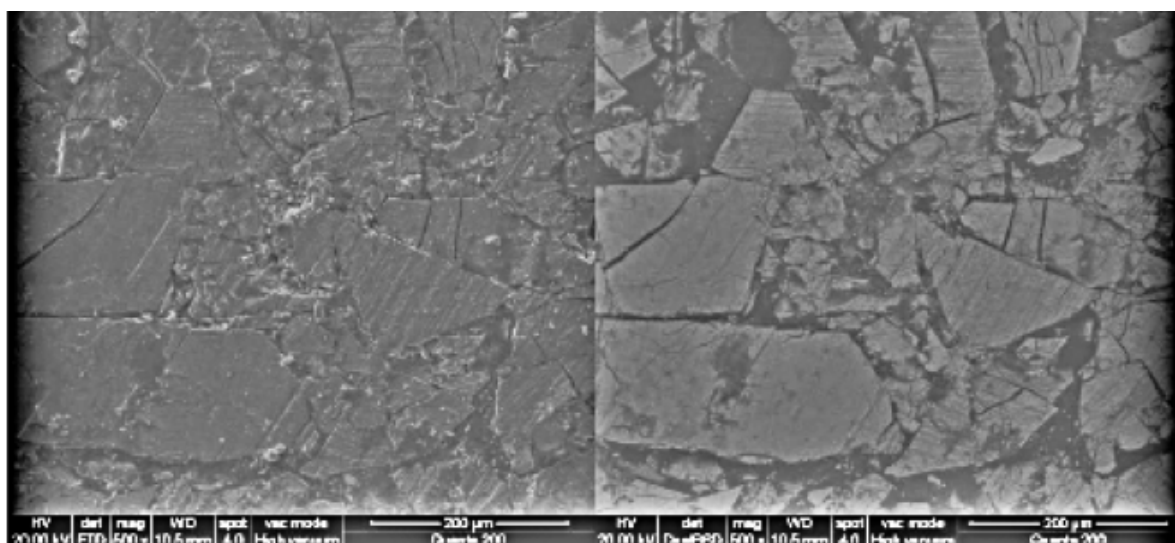


Figure 11. Scanning electron microscopy (left) and backscattered electron microscopy (right) of the bonded magnet surface).

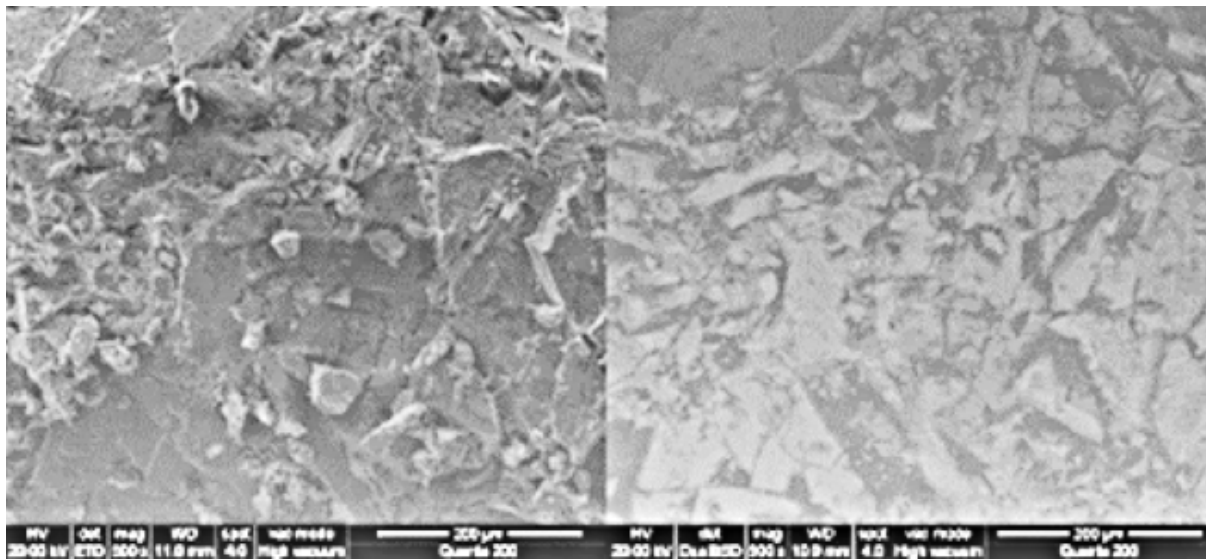


Figure 12. Scanning electron microscopy (left) and backscattered electron microscopy (right) inside the bonded magnet).

3. Principle and Design of Magnetically Controlled Reactor

The nano dual-phase composite magnetic material adopts 1J85 high-performance magnetic material, which has excellent magnetic properties and stability. Based on the characteristics of the rapid response of the nano dual-phase composite magnetic material to the control current and the easy conversion under different magnetic states, a new magnetically controlled reactor structure based on the nano dual-phase composite magnetic material is designed. The two side pillars of the magnetically controlled reactor are the working core pillars, which are composed of the working winding and the silicon steel sheet core. As shown in Figure 13, the middle two columns are control excitation columns, which are composed of the nano dual-phase composite magnetic material and the silicon steel sheet, and the outer side of the nano dual-phase composite magnetic material is wound with control winding.

In the case of reactive power regulation, harmonic suppression or prevention of various faults in the power system, this new type of magnetically controlled reactor can obtain the key physical parameters of the power grid through the control system. These parameters such as voltage, reactive power, and current are then input into the control system. After analyzing the state of the power grid, the control system will formulate a strategy to adjust the remanence of the nano dual-phase composite magnetic material. As shown in Figure 14, the magnetic flux generated by the nano dual-phase composite magnetic material changes after excitation treatment. This change makes the core exhibit different permeability states for different remanence of the nano dual-phase composite magnetic material, which causes the change of the reactance value of the new magnetically controlled reactor. After the system is stable, the control system demagnetizes to make the reactor return to normal working state. This magnetically controlled reactor based on nano dual-phase composite magnetic material can effectively adapt to the dynamic changes of the power grid, thereby improving the overall efficiency and reliability of the power system. Through this advanced technology, the new magnetically controlled reactor can better meet the needs of modern power grids for efficient and intelligent power equipment.

When the magneto control reactor is in operation, the main winding is connected in reverse series, and the main magnetic circuit is the outer ring. As described in the previous material properties, the main magnetic circuit flux does not affect the magnetic flux of the dual-phase composite magnetic material, and thus does not damage the field winding and IGBT.

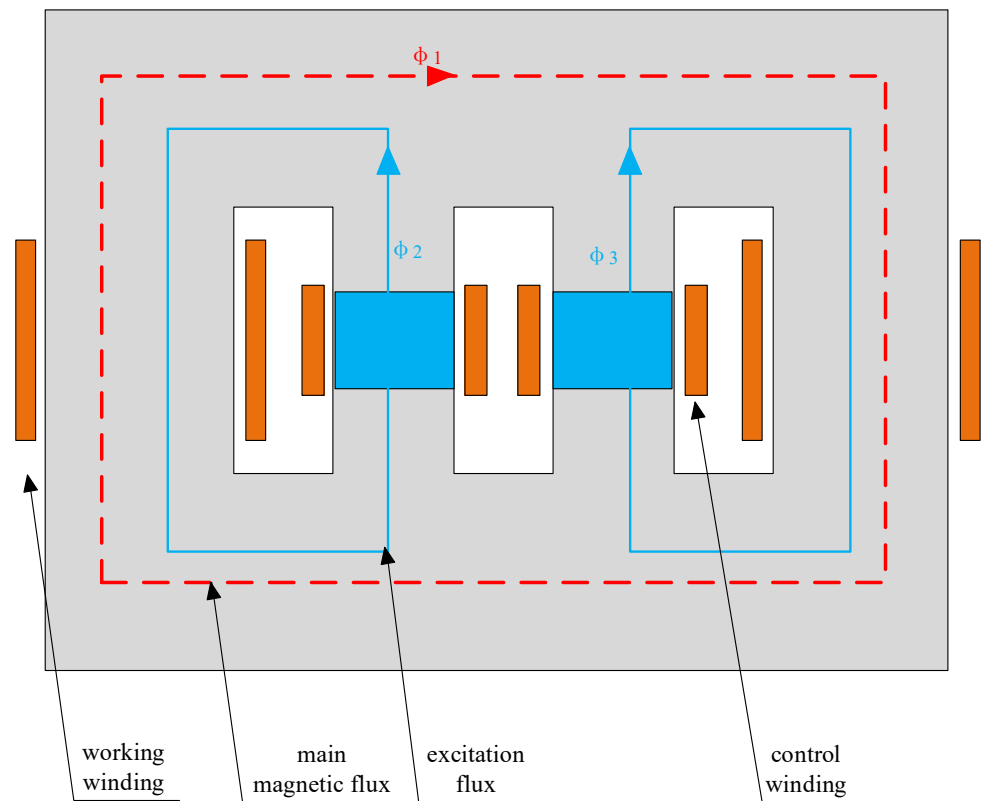


Figure 13. Magnetically controlled reactor structure.

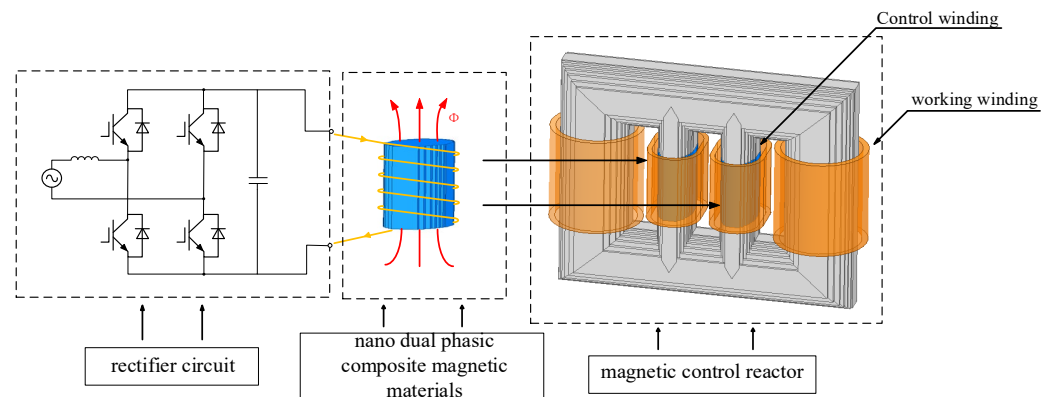


Figure 14. DC excitation working diagram of magnetically controlled reactor.

At the same time, the magnetic control reactor composed of dual-phase composite magnetic materials proposed in this paper only needs a small current in the closed magnetic circuit, which can generate a large magnetic flux, and will not damage the excitation winding and IGBT during the switching process.

Figure 15 shows the schematic diagram of AC/DC pulse hybrid power supply. In the aspect of magnetization, the magnetization magnetic field is realized by obtaining the DC magnetic field through the rectifier circuit. The single-phase full-bridge rectifier circuit adopts neutral point grounding, which can improve the output voltage of the DC attenuation circuit. The parallel voltage plays a role in stabilizing the voltage and can enhance the stability of the system. In terms of demagnetization, the attenuation of the AC magnetic field is realized by an inverter circuit.

Figure 16 shows the block diagram of the single-phase bridge inverter circuit, and the load is a resistance-inductance load. In the bridge inverter circuit, the upper and lower switching devices of the bridge arm are turned on in turn; that is, the on-off states of V1 and V2 are complementary, and the on-off states of V3 and V4 are complementary. Figure 16 shows the three working states of the AC/DC pulse circuit, including forward DC output, reverse DC output, and attenuated AC pulse current output.

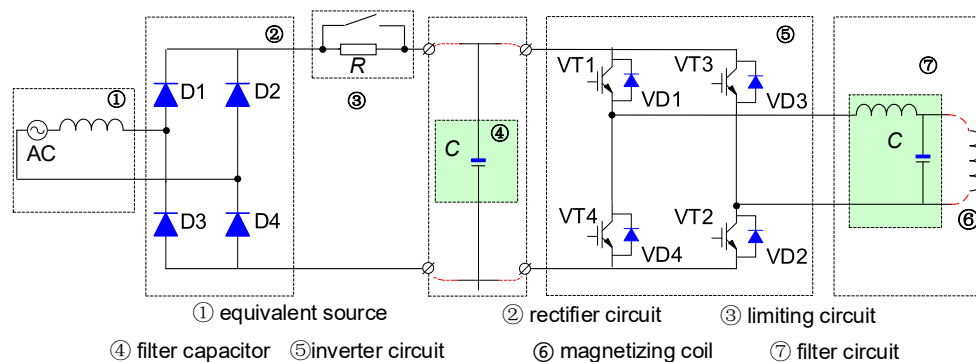


Figure 15. Principle diagram of AC and DC step pulse hybrid power supply.

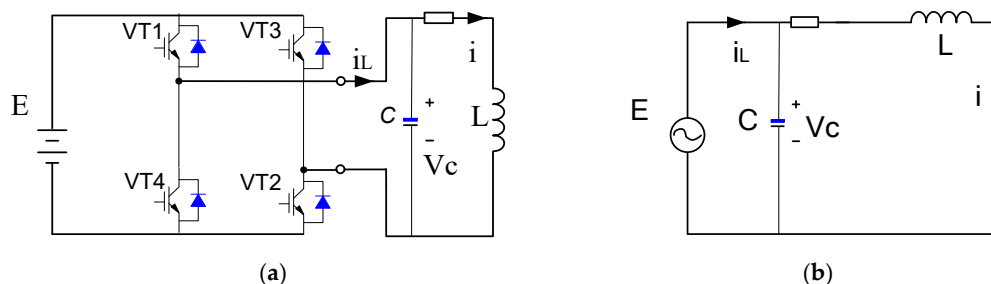


Figure 16. PWM equivalent circuit diagram. (a) Equivalent circuit diagram of single-phase PWM inverter; (b) State circuit diagram of single-phase PWM inverter.

Element 3 is mainly a current limiting circuit. When the control system is powered on, the voltage at both ends of the capacitor cannot change abruptly. If there is no circuit 3, the capacitor will be in a short-circuit state in its initial state. The whole system will not shut down. When circuit 3 is added, the control system is powered on instantaneously, the resistor R plays a current limiting role, so that the capacitor C (4) will not short circuit. When the control system is stable, the switch K is closed, and the resistor bypass is off, so that it does not consume energy.

As shown in Figure 17, D1–D4 consists of a single-phase bridge uncontrolled rectifier circuit. When the input voltage is AC220V, the output DC voltage is about 311 V after diode D1–D4 rectification and capacitor filtering. Therefore, no shunt is required for D1–D4.

Figure 18 shows the amplitude distribution of the system modulation wave, Figure 19 shows the output voltage on the two switch tubes, and Figure 20 shows the distribution of the attenuated alternating current output by the hybrid pulse power supply, which is used for the demagnetization of the composite magnetic material, so that the material is demagnetized to the soft magnetic state without remanence.

Figure 21 shows the simulation results of the magnetization curve.

As shown in Figure 20, the designed two-phase composite magnetic material charging and demagnetization system can output magnetizing voltage and current and demagnetization voltage and current well.

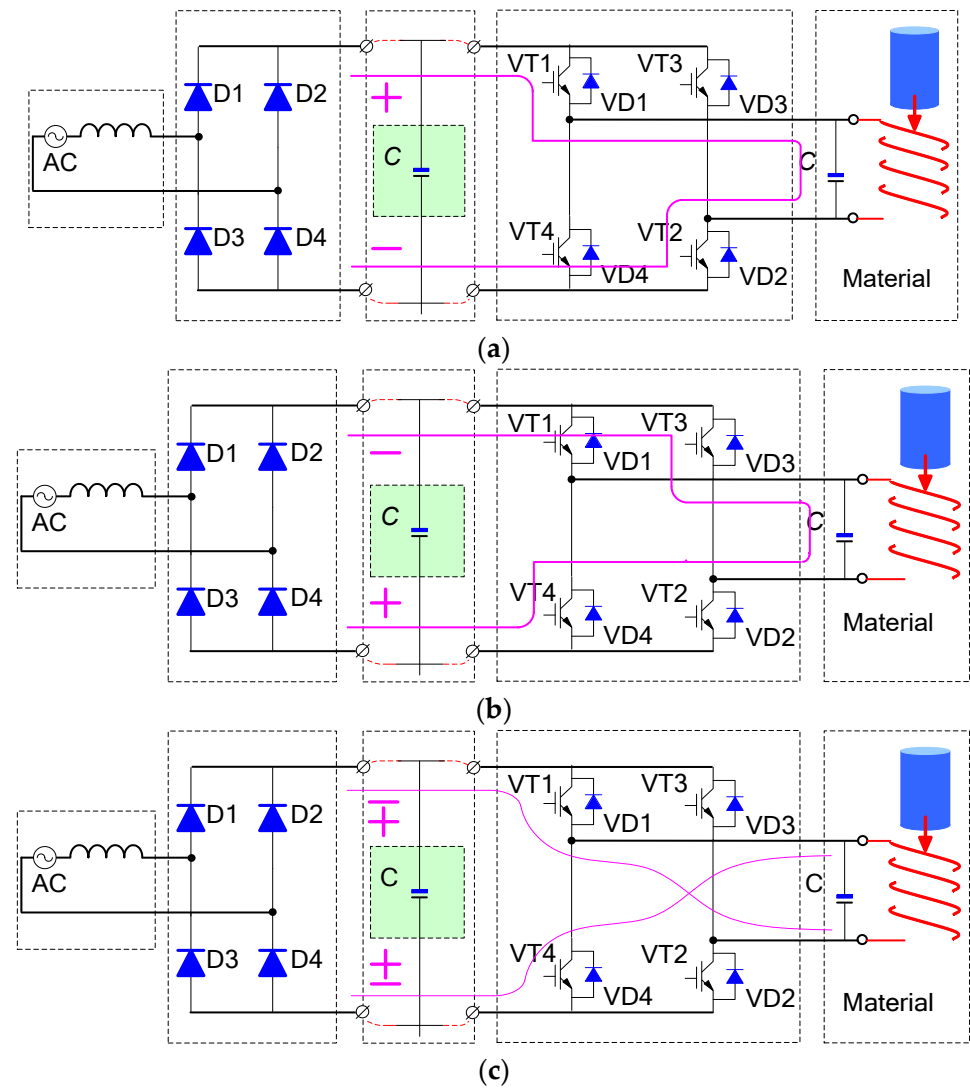


Figure 17. Three circuit working states. (a) Forward current magnetization; (b) Reverse current magnetization; (c) Alternating decay current demagnetization.

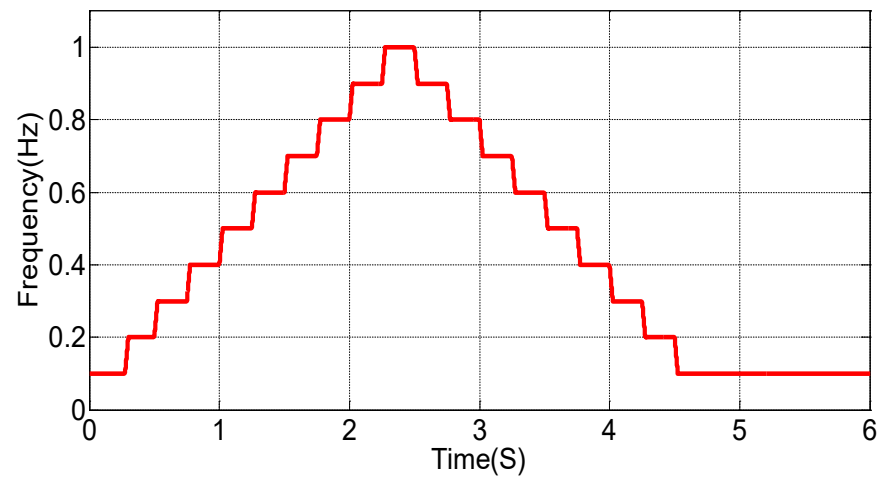


Figure 18. Modulation wave amplitude.

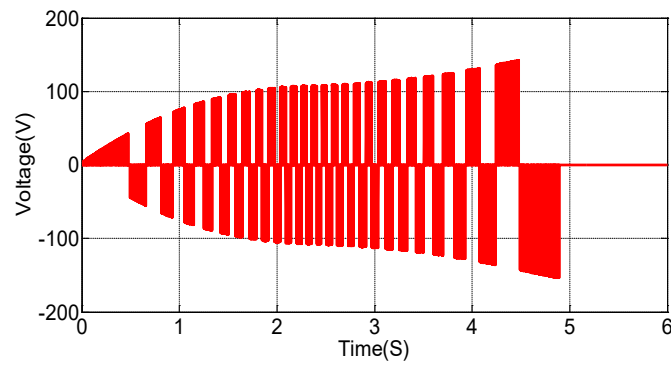


Figure 19. The output voltages on the two switches.

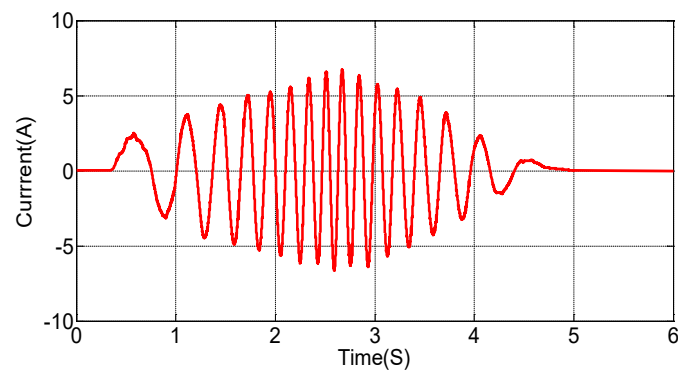
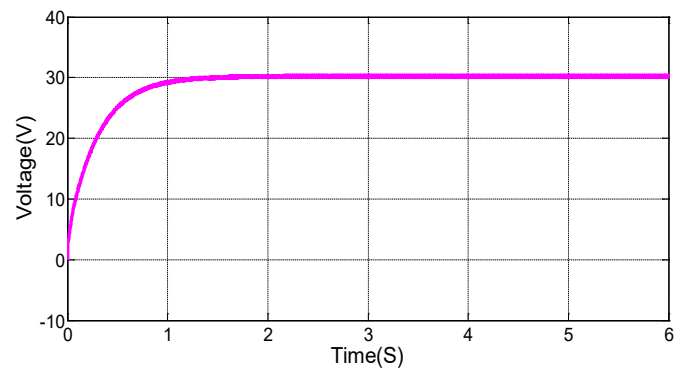
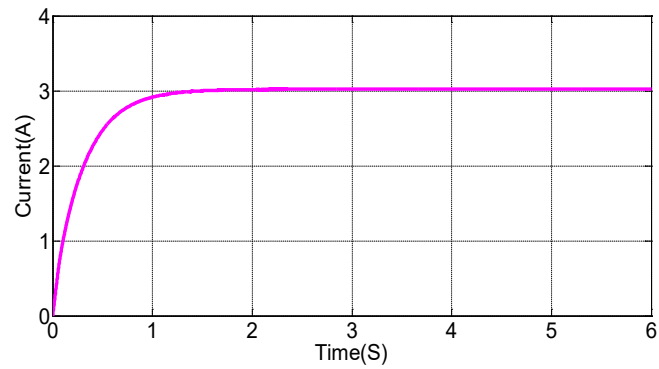


Figure 20. Attenuation AC current curve.



(a) Voltage



(b) Current

Figure 21. The positive DC voltage and current of the magnetizing magnetic field.

There is a set of standards for the design of a magnetically controlled reactor. This paper combines the cost and material level of production to form a set of feasible design methods. In order to improve the magnetic conductivity of the core, it is required that the magnetic flux can be evenly distributed in the core of the reactor. Therefore, the core of the reactor is mostly laminated and pressed by electrical steel sheets. Although the thinner silicon steel sheet is more conducive to the processing of the core and can reduce the eddy current loss, a too-thin silicon steel sheet will also cause the lamination coefficient of the core to decrease. Therefore, in order to reduce the effective magnetic permeability area and reduce the no-load loss, the thickness of the silicon steel sheet is selected to be 0.23~0.35 mm. The core diameter of the reactor is as follows:

$$D_z = KD \cdot \sqrt[4]{S_z} \quad (1)$$

where, KD is the empirical coefficient of core diameter, S_z is the capacity of each column of the reactor.

The net cross-sectional area (effective area) of the core is as follows:

$$A_c = Kd \times A'_c \quad (2)$$

where, A'_c is the geometric area of the multi-stage stepped cross section of the core, and Kd is the core lamination coefficient. In order to improve the overall operating efficiency of the magnetically controlled reactor, the cross-sectional area of the nano dual-phase composite magnetic material is half of the core in the design, which helps to reduce the eddy current loss and improve the magnetic response of the magnetically controlled reactor. The voltage per turn is calculated according to (3):

$$e_0 = 4.44fB_cA_c \times 10^{-4} \quad (3)$$

where, B_c is the maximum working magnetic induction intensity of the core.

The number of winding turns is calculated according to (4):

$$N = \frac{U_{ex}Km}{e_0} \quad (4)$$

where, U_{ex} is the rated phase voltage of the reactor; Km is the voltage drop coefficient.

The winding adopts paper-coated flat copper wire, and the current density is selected as 3.5 A/mm², that is, the cross-sectional area of the wire is calculated.

$$q = \frac{I_x}{j} \quad (5)$$

where, I_x is the winding phase current; j is the current density.

When the number of parallel windings in the amplitude direction is equal to 1, the axial size of a single winding is as follows:

$$B_F = (m + 1)n_2b(K_z/100 + 1) \quad (6)$$

where, m is the number of turns of the full-turn layer, n_2 is the number of parallel wires in the axial direction, B is the size of the insulated wire in the axial direction, and K_z is the axial calculation margin.

The calculation formula of the amplitude dimension of the winding is as follows:

$$B_F = [nn_1a + (n - 1)\delta](K_F/100 + 1) \quad (7)$$

where n is the number of layers; n_1 is the number of parallel wires in the amplitude direction; σ is the thickness of interlayer insulation; K_F is the margin of amplitude calculation.

From the above calculation, the design parameters of the magnetically controlled reactor based on the nano dual-phase composite magnetic material are shown in Table 7.

Table 7. Design parameters of 380 V/100 kVA magnetically controlled reactor.

Item	Parameter	Value
basic parameter	rated voltage	380 V
	rated capacity	100 kVA
core parameter	diameter	180 mm
	cross-sectional area	18,215 mm ²
composite material parameters	height	80 mm
	cross-sectional area	9108 mm ²
winding parameter	wire type	paper-wrapped flat copper wire
	turns of working winding	96
	control winding turns	70
	amplitude dimension of winding	10 mm
	axial dimension of working winding	207 mm
	control winding axial dimension	98 mm

4. Magnetic Field Simulation of Magnetically Controlled Reactor

Figure 22 shows the magnetic induction intensity distribution of the core of the magnetically controlled reactor when the remanence of the nano dual-phase composite magnetic material is 0.3 T, 0.6 T, and 0.9 T, respectively. The magnetic state of the nano dual-phase composite magnetic material can be adjusted and the remanence of the nano dual-phase composite magnetic material can be controlled by changing the current. The homonymous ends of the control windings on the left and right sides are in parallel, so that the remanence flux generated by the nano dual-phase composite magnetic material on the left and right sides is in the same direction, forming a closed loop with the adjacent iron core. Because the cross-sectional area of the core is twice that of the nano dual-phase composite magnetic material, the magnetic induction intensity in the nano dual-phase composite magnetic material is twice that of the core magnetic induction intensity, which improves the remanence of the nano dual-phase composite magnetic material. This also leads to more accurate control of the magnetic induction intensity of the main magnetic circuit. With the gradual increase in the remanence flux density of the nano dual-phase composite magnetic material, it shows that the material can achieve a high magnetization level and relatively low coercivity. This means that the material can easily reach the required magnetization level and can be effectively demagnetized. Through the continuous adjustment of the remanence of the nano dual-phase composite magnetic material, the inductance value of the magnetically controlled reactor is adjusted more smoothly, so that the power line can be quickly compensated for reactive power. This means that in power lines, reactive power compensation can be more accurately controlled to meet the needs of different loads and operating conditions, which is essential for maintaining the stability and efficiency of the power system. By understanding the magnetic properties of the material and making full use of its performance in the magnetically controlled reactor, more efficient, adjustable, and stable power lines can be achieved to meet the changing power demand. This provides strong support for technological progress in the power sector and is expected to improve the performance and stability of the power system.

The adjustment of the inductance of the magnetically controlled reactor based on the nano dual-phase composite magnetic material is achieved by changing the current value of the control winding to change the remanence of the nano dual-phase composite magnetic material, thereby changing the core saturation. Therefore, in order to obtain the accurate electromagnetic characteristics of the magnetically controlled reactor, it is necessary to input the AC voltage to the working winding and input the DC current to the control winding to obtain the electromagnetic characteristics of the magnetically controlled reactor under different remanence. It can be seen from Figure 23a that the magnetic induction intensity of the right core column of the magnetically controlled reactor is the largest, followed by the

nano dual-phase composite magnetic material and the left core. This is because the working winding of the magnetically controlled reactor generates clockwise magnetic flux in the core columns on both sides, and the control winding of the magnetically controlled reactor generates upward DC magnetic flux in the nano dual-phase composite magnetic material; the control winding of the magnetically controlled reactor produces DC magnetic flux in the same direction as the magnetic flux of the working winding in the right core column. Therefore, the magnetic flux in the same direction acts on the right core column, which makes the magnetic flux density of the right core column increase. The magnetic flux in the left core column flows through two opposite directions, and the magnetic flux density increases. Similar to Figure 23b,c, the magnetic flux generated by the control winding and the working winding in the left core is reversed, the magnetic flux generated by the control winding and the working winding in the right core is in the same direction, and the demagnetization of the left core column and the magnetization of the right core column. With the increase in the remanence of the nano two-phase iron composite magnetic material, the magnetic flux density of the left core column gradually decreases, and the magnetic flux density of the right core column gradually increases. The simulation results show that the change of remanence has a significant effect on the electromagnetic characteristics of the magnetically controlled reactor. The remanence can be changed by adjusting the current of the control winding, so as to effectively adjust the inductance of the magnetically controlled reactor.

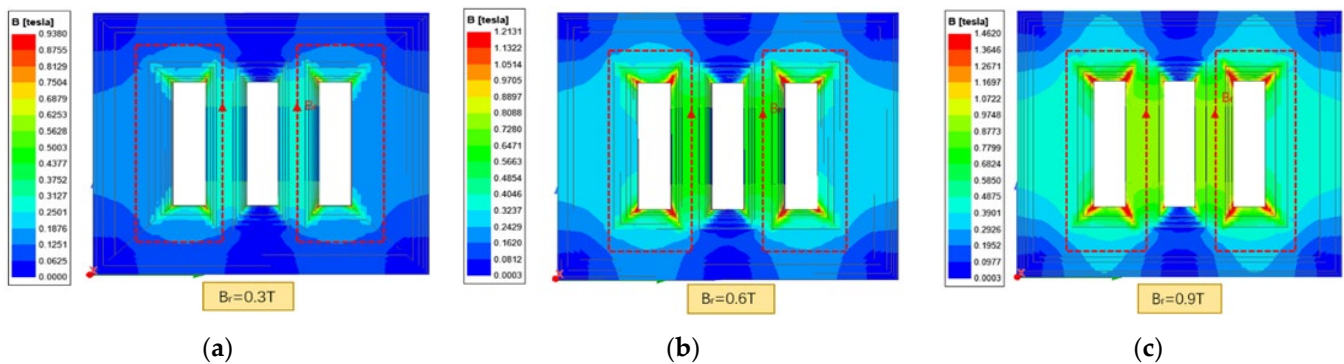


Figure 22. Magnetic induction intensity of core of nano two-phase magnetic material under different remanence: (a) $B_r = 0.3$ T; (b) $B_r = 0.6$ T; (c) $B_r = 0.9$ T.

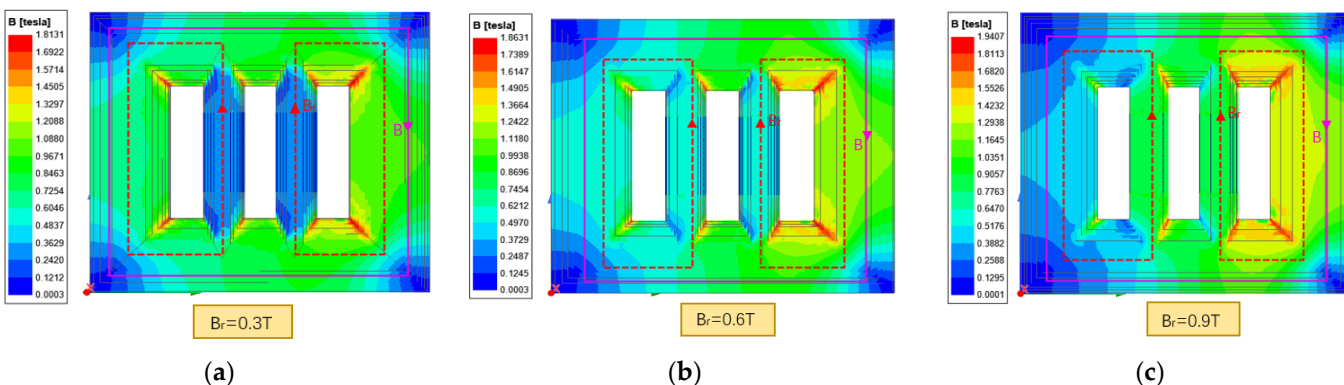


Figure 23. The magnetic induction intensity of the core under normal operation of the magnetically controlled reactor: (a) $B_r = 0.3$ T; (b) $B_r = 0.6$ T; (c) $B_r = 0.9$ T.

5. Characteristic Analysis of Magnetically Controlled Reactor

The control characteristic of the magnetically controlled reactor is that the effective value of the working winding current increases linearly with the increase in the remanence of the nano dual-phase composite magnetic material, as shown in Figure 24. This makes it

possible to control the inductance of the magnetically controlled reactor more accurately within a certain range. In order to make the control characteristics of the magnetically controlled reactor more accurate, it is necessary to calculate the effective value of the working winding current under different remanence of the nano dual-phase composite magnetic material. The finite element method can only obtain the working winding current waveform, and the effective value of the working winding current cannot be directly obtained. Therefore, this paper uses the equation (8):

$$I = \sqrt{\frac{1}{T} \int_0^T i^2 dt} \quad (8)$$

where, i is the working winding current value calculated by finite element method. T is the working winding current waveform cycle, I is the effective value of the working winding current.

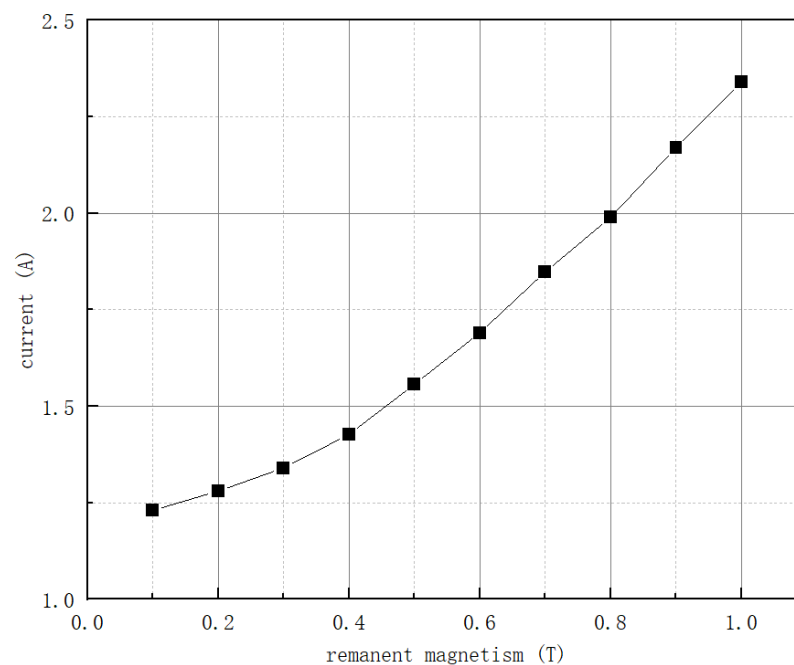


Figure 24. Control characteristic.

The current value of the working winding in a cycle under different control currents is integrated by software, and the integral result is substituted into the formula to calculate the effective value of the working winding current under different remanence of the nano dual-phase composite magnetic material.

The volt-ampere characteristic curve of the magnetically controlled reactor shows the corresponding relationship between the effective value of the working winding voltage and the effective value of the working current under different remanence of the nano dual-phase composite magnetic material. Figure 24 shows that when the remanence of nano dual-phase composite magnetic material is 0.6 T, 0.7 T, 0.8 T, 0.9 T, and 1 T, the finite element calculation obtains the current value of the working winding under different working winding voltages. The current of the working winding of the magnetically controlled reactor increases linearly with the increase in the applied voltage value, indicating that the inductance value is relatively constant under different remanence, does not change greatly with the change of voltage and current, and its volt-ampere characteristic curve is relatively stable. Figure 25 is the curve of inductance changing with magnetizing voltage. It can be seen that the inductance output of the magnetically controlled reactor is stable, and the goal of smooth adjustment of the reactor is completed.

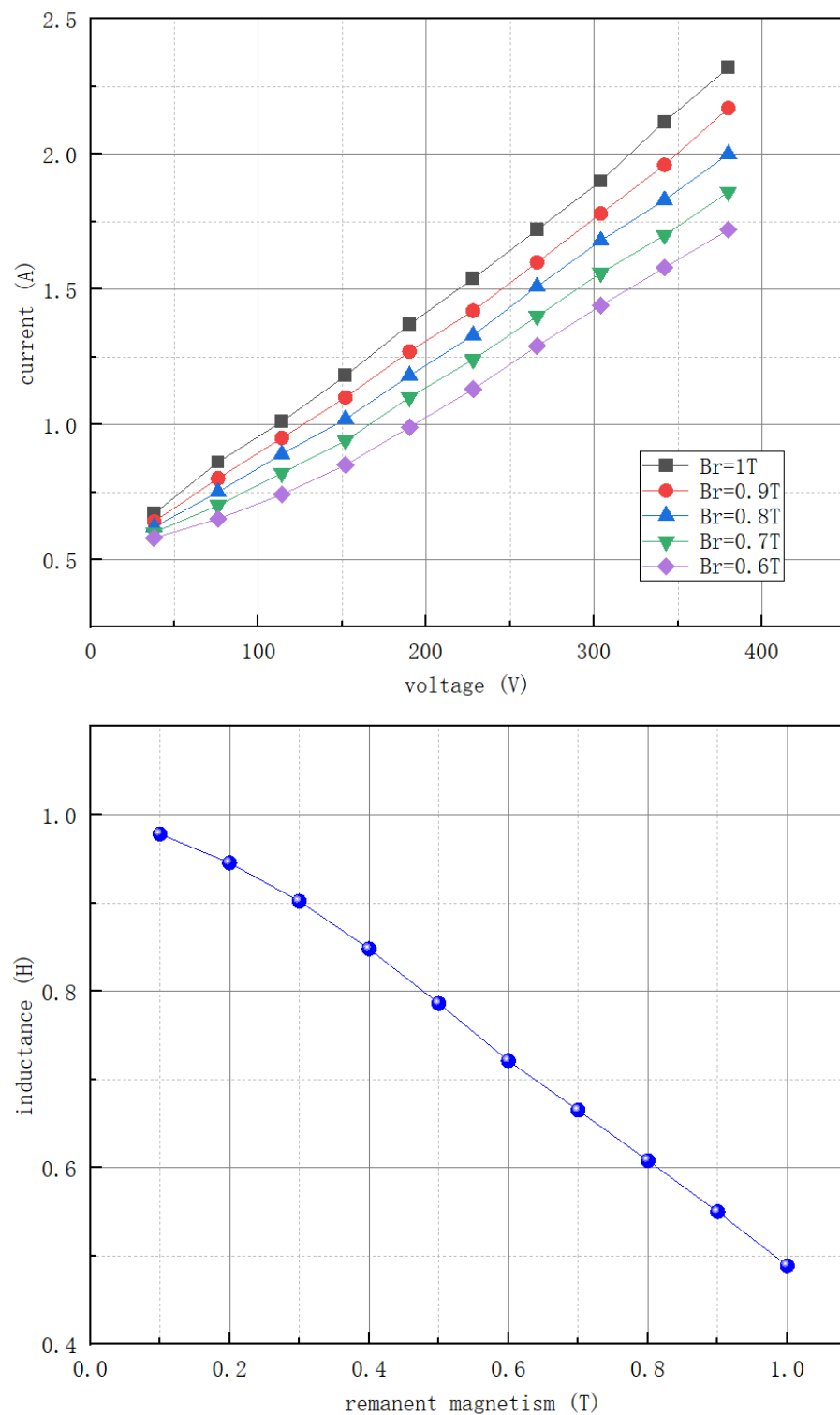


Figure 25. Curve of inductance changing with magnetizing voltage.

6. Conclusions

A two-phase composite magnetic material and its preparation method are proposed in this paper. Based on the magnetic properties of this material, it is applied to the magnetically controlled reactor. A 380 V/100 kvar new magnetically controlled reactor and its control system are designed. The relevant simulation and experimental research are carried out, and the following conclusions are obtained:

- (1) Based on $f[\text{Nd}_{1-x}\text{La}_x]_8\text{Fe}_{86}\text{B}_6$ ($x = 0.3, 0.4$), the preparation of dual-phase composite magnetic materials was carried out by melt-spinning method. The metal content ratio, processing technology, and heat treatment process were studied, and the magnetic properties were tested. The dual-phase composite magnetic materials with low coercivity and high remanence were successfully prepared.
- (2) An AC/DC hybrid power supply topology and control method are proposed. The DC magnetization and AC attenuation pulse demagnetization of the two-phase composite magnetic material are realized. The specific design process and simulation results are given.
- (3) Based on the conversion characteristics of dual-phase composite magnetic material between soft magnetic and permanent magnetic, a new type of dual-phase magnetic controlled reactor structure is proposed by applying it to magnetic controlled reactor. The specific design process is given, and its electromagnetic characteristics and volt-ampere characteristics are simulated and analyzed to verify the correctness of the proposed scheme.

The prototype of the magnetic control reactor based on dual-phase composite magnetic materials and the system experiment are under development and will be presented in the pages of *Energies* in the future.

Author Contributions: Conceptualization, Y.L.; methodology, F.Y.; software, Y.H.; validation, J.G.; formal analysis, C.W.; investigation, D.C.; data curation, H.B.; writing—original draft preparation, Y.L. and Y.H.; writing—review and editing, Y.L. and Y.H. All authors have read and agreed to the published version of the manuscript.

Funding: This work was financially supported by the Science and Technology Project of State Grid Corporation of China (5500-202258312A-2-0-QZ).

Data Availability Statement: The original contributions presented in the study are included in the article, further inquiries can be directed to the corresponding author.

Conflicts of Interest: Authors Yang Liu, Fuyao Yang, Yu Han, Jie Gao, Cong Wang, were employed by the State Key Laboratory of Advanced Power Transmission Technology and State Grid Smart Grid Research Institute Co., Ltd. Authors Dezhi Chen and Haonan Bai were belong to Shenyang University of Technology. The remaining authors declare that the research was conducted in the absence of any commercial or financial relationships that could be construed as a potential conflict of interest.

References

1. Fouda, S.S.; Salama, M.M.A.; Chikhani, A.Y. Characteristic Performance of Thyristor Controlled Reactor Used in Reactive Power Control. In Proceedings of the Canadian Conference on Electrical and Computer Engineering, Vancouver, BC, Canada, 14–17 September 1993; IEEE: Piscataway, NJ, USA, 1993; pp. 445–448.
2. Cai, X.; Gao, Y. *Principle, Design and Application of Controllable Saturable Reactor*; Water Conservancy and Hydropower Press: Beijing, China, 2008.
3. Liu, W.; Luo, L.; Dong, S.; Lou, Y. The Summarize of Power Controllable Reactor Technology. In Proceedings of the Conference on PEITS 2010, Shenzhen, China, 13–14 November 2010; IEEE: Piscataway, NJ, USA, 2010; pp. 29–33.
4. Gu, S.; Tian, M. Research and Development of Transformer Type Controllable Reactor. *High Volt. Appar.* **2014**, *50*, 20–23.
5. Mou, H.; Wang, J.; Ji, Y.; Wei, X. Current Status and Development of Controllable Reactors. *Electr. Appl.* **2006**, *25*, 1–4.
6. Yu, M.; Chen, B.; Cao, Z.; Tian, C.; Qiu, H. 110 kV Shunt Controllable Reactor and Its Application. *Power Syst. Autom.* **2008**, *32*, 87–91.
7. Sundar, S.V.N.J.; Vaishnavi, G. Performance Study of a Continuously Controlled Shunt Reactor for Bus voltage Management in EHV systems. In Proceedings of the International Conference on Power Systems Transients, Lyon, France, 4–7 June 2007.
8. Yury, I.; Martirosyan, A. The development of the Soderberg electrolyzer electromagnetic field's state monitoring system. *Sci. Rep.* **2024**, *14*, 3501. [[CrossRef](#)] [[PubMed](#)]
9. Yin, Z.; Cheng, X.; Liu, H. Application of Controllable Reactor in Automatic Compensation of Capacitive Current in Power Grid. *High Volt. Technol.* **1996**, *22*, 85–87.
10. Zhou, Q.; Guo, Q.; Bu, G.; Ban, L.-G. Application of controllable reactor in UHV power grid in China. *Chin. J. Electr. Eng.* **2007**, *27*, 1–6.
11. Li, D.; Chen, Q.; Jia, Z. New principle of adjustable reactor based on controllable magnetic flux. *Chin. J. Electr. Eng.* **2003**, *23*, 116–120.

12. Dolgoplova, G.; Dolgoplov, G.; Zaitseva, L.; Shipitsin, V.P. Industrial Operation of a Controllable Three-Phase Shunting Reactor(110 kV, 25000 kVA) at the Permenergo Kudymkar Substation. *Russ. Electr. Eng.* **2003**, *74*, 29–34.
13. Yan, A.; Cheng, S.; Li, L.; Fang, L.; Liu, S. Controllable reactor and its application in soft starting of asynchronous motor. *Explos. Proof Mot.* **2008**, *43*, 26–28.
14. Ichinokura, O.; Maeda, M.; Sakamoto, M.; Mitamura, K.; Ito, T.; Saito, T. Development of 3-phase 100 kVA orthogonal-core type variable inductor with sinusoidal output. *IEEE Trans. Magn.* **1998**, *34*, 2066–2068. [[CrossRef](#)]
15. Hua, J.; Goos, G.; Lopes, L. An efficient switched-reactor-based static var compensator. *IEEE Trans Ind. Appl.* **1994**, *30*, 998–1005.
16. Zhao, G.; Li, P. The Characteristics Analysis of Controllable Reactor of Transformer Type. In Proceedings of the 2019 IEEE Innovative Smart Grid Technologies—Asia (ISGT Asia), Chengdu, China, 21–24 May 2019; pp. 4231–4234. [[CrossRef](#)]
17. Wang, Z.; Tang, Y.; Ren, L.; Yan, S.; Shen, S.; Xu, Y.; Hu, N.; Zhang, C. Performance Analysis and Prototype Design of a D-Core-Type Single-Phase HTS Controllable Reactor. *IEEE Trans. Appl. Supercond.* **2016**, *26*, 0603304. [[CrossRef](#)]
18. Wang, W.; Xie, X.; Yin, H.; Li, D.; Li, J. Research on A Controllable Reactor Realized by Multi-Winding Transformer. In Proceedings of the 2023 3rd Power System and Green Energy Conference (PSGEC), Shanghai, China, 24–26 August 2023; pp. 950–954. [[CrossRef](#)]
19. Liu, G.-M.; Wu, D.-F. Effects and measurements of current differential protection for transmission line with transformer type controllable shunt reactor. In Proceedings of the 2016 IEEE Power and Energy Society General Meeting (PESGM), Boston, MA, USA, 17–21 July 2016; pp. 1–9. [[CrossRef](#)]
20. Zhang, Y.; Li, J.; Wang, Z.; Yan, S.; Ren, L.; Xu, Y.; Tang, Y. Saturation and Hysteresis Characteristics Analysis of a HTS Controllable Reactor with Orthogonally Configured Core. *IEEE Trans. Appl. Supercond.* **2019**, *29*, 5001105. [[CrossRef](#)]

Disclaimer/Publisher’s Note: The statements, opinions and data contained in all publications are solely those of the individual author(s) and contributor(s) and not of MDPI and/or the editor(s). MDPI and/or the editor(s) disclaim responsibility for any injury to people or property resulting from any ideas, methods, instructions or products referred to in the content.